Research Article

Greg W. Forbes*, Johannes Ruoff*, Andreas Flesch and Norbert Kerwien

Ray selection for optimization of rotationally symmetric systems

DOI 10.1515/aot-2016-0019
Received March 24, 2016; accepted April 21, 2016; previously published online May 16, 2016

Abstract: Efficient performance assessment is essential during the design of systems involving complex aspheres. We present new classes of pupil sampling schemes that, with a reduced number of rays, yield accurate estimates of the RMS wavefront aberration over a circular pupil. It turns out that the number of samples in the pupil can be reduced by a factor of about 0.7, and these ideas can also be expected to lead to a similar additional reduction factor when averaging over the field and color. Beyond that, analysis of a patented lens system is used to establish the path to further significant reductions.

Keywords: aspheres; cubature; optical design; optimization.

1 Introduction

When compared to traditional designs, the application of increasingly complex aspheres means that additional rays must be traced to estimate merit functions with sufficient accuracy. It is otherwise possible to achieve high levels of correction for the sampled rays while permitting poor performance within the unsampled regions of the pupil. Despite the ongoing boom in computing power, efficiency is crucial in these challenging design tasks when there are many active degrees of freedom. Optimal ray sampling, therefore, remains critical. We focus in this work upon axially symmetric systems and accept that entities like the RMS over the pupil of the geometrical-optics-based wave aberration involve underlying approximations that set a limit to meaningful accuracy. In at least the initial phases of design, however, such averages provide valuable figures of merit.

For averaging over the pupil, earlier work in this area applied Gaussian quadrature separately in angle and radius [1]. This approach is sometimes referred to as 'iterated Gaussian quadrature' (IGQ) and is effective for lower orders of correction. Unfortunately, it is not optimally matched to the task for high-performance systems where larger numbers of samples are required for averaging both the wavefront aberration and its square. Although explanation of their classification is delayed until Section 2, it is apparent in Figure 1 that these sampling patterns for higher-order schemes become unevenly bunched.

Although it appears to be not well known in the optical design context, there is an existing body of work on what is referred to as 'cubature'. This is reviewed in Ref. [2] and includes specific schemes for estimating uniformly weighted averages over a disc [3]. An online encyclopedia is also partially assembled (see [4]). The sampling scheme from the encyclopedia for order 25 is shown in Figure 2 where it is evident that some of the uneven bunching at the right in Figure 1 has been reduced, and the number of samples has fallen by 15–20%. A variety of such schemes exist, and some more attractive and effective options form the subject of this paper. We present one approach for deriving these schemes in Section 2 and some sample solutions in Section 3 before considering a key application in Section 4 that points the way to further significant improvements.

2 Symmetric cubature schemes

When polynomials are able to approximate the integrands of interest, it is natural to apply quadrature schemes that use a linear combination of a finite number of samples designed to exactly integrate as many monomial terms as possible. For the estimation of one-dimensional integrals over a finite interval, Gaussian quadrature manages to

***Corresponding authors: Greg W. Forbes,** Physics Department, Macquarie University, North Ryde 2109, Sydney NSW, Australia, e-mail: forbes@bigpond.net.au; and **Johannes Ruoff,** Carl Zeiss SMT GmbH, Rudolf-Eber-Strasse 2, 73447 Oberkochen, Germany, e-mail: johannes.ruoff@zeiss.com
Andreas Flesch and Norbert Kerwien: Carl Zeiss AG, Carl-Zeiss-Strasse 22, 73447 Oberkochen, Germany

www.degruyter.com/aot

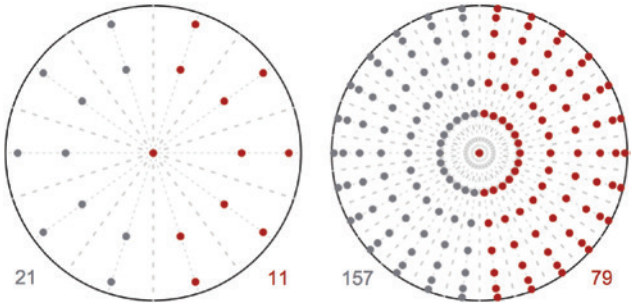

Figure 1: IGQ schemes for order 9 at the left and order 25 at the right (with 11 and 79 samples). Only half of the pupil needs to be sampled due to symmetry. The number of samples in the full disc is also shown in gray.

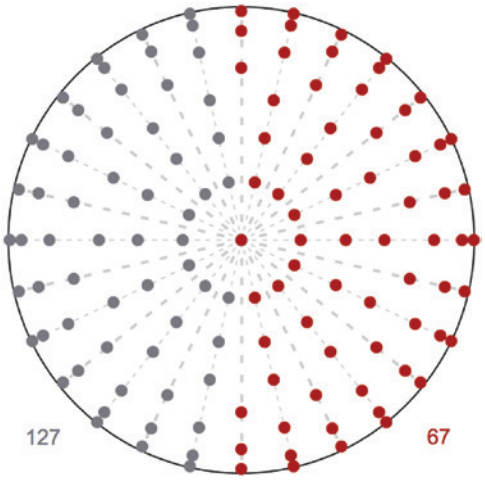

Figure 2: A long known cubature scheme for order 25. Here, 67 samples in only half of the 14 (internally symmetric) sectors are required due to symmetry.

integrate polynomials up to the order $2n$-1 by using only n sample points: There are $2n$ degrees of freedom in the sample locations and weights, and this is also the number of monomial terms in the target polynomial. It so happens that the associated set of $2n$ non-linear equations (one for each of the monomials) that involve these $2n$ unknowns always has a beautiful solution where the sample locations all fall within the interval of integration [normalized here to (-1,1)], and all the weights are positive. Unsurprisingly perhaps, those sample locations and weights are symmetric about the origin. Anti-symmetric terms, therefore, sum precisely to zero; hence, it is an even term, namely, the order $2n$, which is the first to fail.

For integrating over the unit disc in terms of Cartesian coordinates (x,y), it turns out to be effective for general purposes to attempt to integrate all the monomials $x^j y^k$ up to a fixed order, say t, where $t=j+k$. This follows from the observation (evident in the domain of orthogonal polynomials, see Sec. 6.1 of [5]) that smooth functions that exhibit variations on a scale that allow up to about C cycles across the domain are predominantly captured by terms up to the order $t\approx\pi C$. For simplicity, only symmetric sampling schemes are investigated here. That is, as is the case in Figures 1 and 2, we consider only configurations where the samples are invariant under sign changes of x and y. All terms involving any odd orders are then automatically handled exactly, and just as for Gaussian quadrature, the resulting schemes are, therefore, designed to integrate all terms up to, and including some, fixed odd value of t. Because the integrands of interest to us are symmetric functions of x, the desired integral is then just twice the integral over the semi-circle where $x\geq 0$. Also notice in the figures above that, if the sample points are reflected into $x<0$ to fill the whole disc and the resulting grid is rotated by $\pi/2$, an alternative configuration results. In each of these three cases, however, a greater number of samples is now required within $x\geq 0$. This is because there are then more points on the y axis. Accordingly, we rotate all solutions to ensure a minimal number of samples on that vertical line of symmetry.

As a benchmark, consider the application of IGQ in polar coordinates for integrating all terms up to an odd order, say $t=2h+1$. It can be seen that we must sample on $h+1$ spokes. The samples then sit on $(h+1)/2$ rings when h is odd or on $h/2$ rings with an additional sample at the centre when h is even. (As shown in Figure 1, the Radau variant of Gaussian quadrature is used when h is even.) As each sample generally brings three degrees of freedom (two for location and one for weight), the number of samples required by a cubature scheme can be estimated to be one third of the number of terms $x^j y^k$ with even values of j where $j+k\leq t$, i.e. one third of $(t+3)(t+1)/4$. For large h – hence large t – it follows that Gauss requires $t^2/8+O(t)$ samples, while this simple estimate for cubature is about 33% less, namely, $t^2/12+O(t)$. A comparison for moderate orders is presented in Table 1.

2.1 Configuring specific schemes

Cubature schemes are designed to estimate an integral as a linear combination of function values, say

$$\int f(x)dx \sim \sum_i w_i f(x_i). \tag{1}$$

For a given number of samples, the goal is to determine sample locations and weights that give exact results up to the highest polynomial order possible. That challenge can be taken on by minimizing the sum of the squared error resulting in Eq. (1) when summed over any

Table 1: A comparison of the number of samples required in a semi-circle by iterated Gaussian quadrature and a simple estimate of the number required by cubature.

t	# IGQ	# CubEst	% Reduction
11	18	14	22.2
13	22	56/3	15.2
15	32	24	25.0
17	37	30	18.9
19	50	110/3	26.7
21	56	44	21.4
23	72	52	27.8
25	79	182/3	23.2
27	98	70	28.6
29	106	80	24.5
31	128	272/3	29.2
33	137	102	25.5
35	162	114	29.6
37	172	380/3	26.4
39	200	140	30.0
41	211	154	27.0
43	242	506/3	30.3

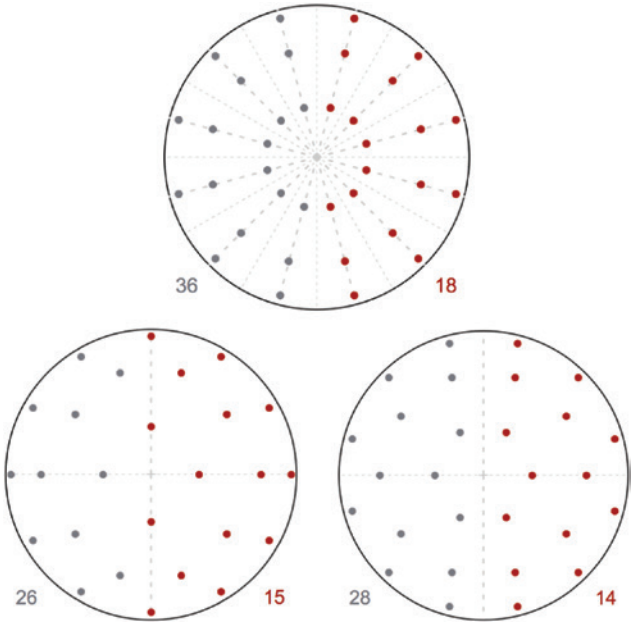

Figure 3: IGQ scheme for order 11 at the top, and two cubature options for order 11 below.

target set of basis functions, say monomials or orthogonal polynomials. As the weights appear linearly in these errors, they can be determined via standard linear least squares methods. This reduces the task to the optimization of just the sample locations. (Note that, after the weights have been determined, the merit function is best left in the form of a sum of squares in order to reduce round-off effects.) Ultimately, solutions are rejected if any of the weights are negative or any samples fall outside the region of integration.

We applied a variety of simple optimization schemes (including conjugate gradient, damped least squares, and other canned algorithms) to arrive at the results presented below. While monomials are an acceptable basis in this work either for low-order solutions or for the initial phases of optimization, it is numerically preferable to use orthogonal polynomials to avoid catastrophic round-off complications. In particular, we adopted the symmetric Zernike polynomials given in terms of the Jacobi polynomials as

$$Z_n^m(r,\theta)=r^m \cos m\theta P_n^{(0,m)}(2r^2\text{-}1). \tag{2}$$

Simple trigonometric identities establish that $Z_n^m(r,\theta)$ is a polynomial of order $t=2n+m$ in the Cartesian coordinates. In fact, when supplemented with the anti-symmetric Zernikes (where cos is replaced by sin), the set of all terms with $m+2n\le t$ is exactly interchangeable with the monomial terms x^jy^k, where $j+k\le t$. This result follows from the discussion of Eq. (6) in Ref. [6]. Orthogonality means that $Z_n^m(r,\theta)$ integrates to zero unless $m=n=0$, so Eq. (1) becomes especially simple, and those requirements are then numerically robust provided recurrence relations are used to evaluate the Jacobi polynomials.

3 Examples of moderate-order configurations

This task has now been reduced to the optimization of the location of a set of points in the unit semi-circle. A selection of configurations is offered in this section to give an idea of the varieties of solutions that emerge. Some numerical details are presented in the Appendix.

3.1 Order 11

In this case, $h=5$ and IGQ needs six spokes of three rings for a total of 18 sample points. The result is shown in Figure 3 along with two cubature schemes for order 11. There are 15 samples at the bottom left in Figure 3 and 14 samples at the bottom right, and the latter matches the simple estimate given in Table 1. It turns out that there is a one-parameter family of solutions for both these cubature options; the cases displayed have the three most central samples chosen to be equidistant from the origin.

More generally, the most central point on the horizontal axis is free to move side to side (over a narrow range), while the other samples and weights adapt to maintain the state of correction. That is, there is one superfluous degree of freedom. (There are 22 degrees of freedom in each of these schemes and only 21 terms with even powers of x and y.) Notice that when the integrand is not symmetric, each of these configurations must be reflected to fill the left side of the disc making a more general 11th-order cubature scheme with 26 and 28 samples, respectively. Because it then has more samples, this means that the 14-sample scheme would not feature in the traditional literature on cubature, but it is the preferred one in our context, where it represents a 22% reduction over IGQ.

3.2 Order 25

The reference list in Ref. [4] establishes that the cubature scheme for order 25 that was presented in Figure 2 was first reported at least 40 years ago. Because the weights are uniform for the 14 points around each ring, all the sampled Zernikes sum exactly to zero except for the 13 terms with m=0 and the 6 terms with m=14. (Recall $m+2n \le 25$.) These, therefore, comprise the 19 basis elements used in the analog of Eq. (1) for this case. To satisfy these 19 requirements, there are six coordinates for the points along the positive x axis and three coordinates for the points on the line at angle $\pi/14$ making 9 degrees of freedom. These supplement the 10 weights to give a total of 19 degrees of freedom that makes a solution seem viable although not necessarily guaranteed. Optimization of such a configuration, however, readily leads to the solution shown in Figure 2 with 67 samples over the semi-circle in place of the 79 samples for the corresponding IGQ in Figure 1 (i.e. only a 15% reduction).

Although the resulting sampling pattern in Figure 2 is more attractive, the shape of the perimeter still appears to be awkwardly dictating the geometry of the sampling near the center. It seems natural, therefore, to seek a solution where the sampling near the center is a more uniformly distributed set of points with roughly uniform weights. More importantly, the simple estimate in Table 1 suggests that we may be able to find a solution with closer to 60 samples instead of the 67 in Figure 2.

When we drop from the 14-fold symmetry in Figure 2 down to the sixfold symmetry, $Z_n^m(r,\theta)$ then sum exactly to zero except when m=0, 6, 12, 18, and 24, where there are 13, 10, 7, 4, and 1 terms, respectively, within $m+2n \le 25$ making a total of 35 requirements to be met. Aside from the origin, the sampling scheme at the upper left in Figure 4

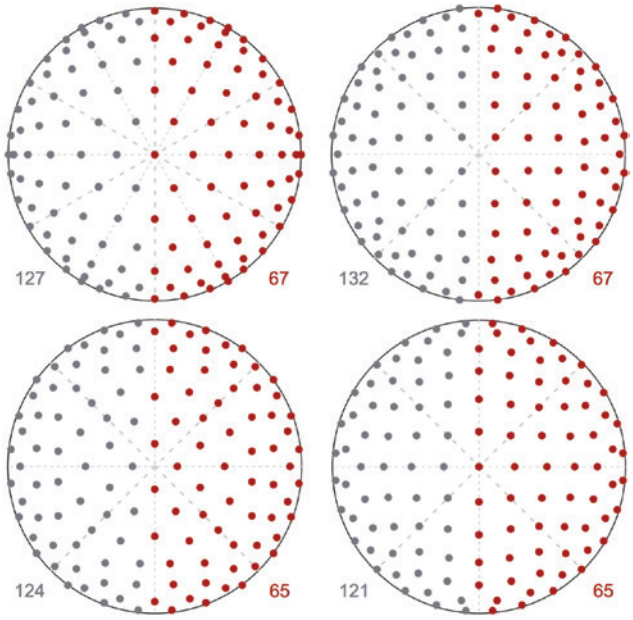

Figure 4: A selection of novel cubature schemes for order 25. The example at the lower right has 65 samples in the semi-circle and 121 when the integrand is not symmetric.

has six points on the positive x axis and three on the line at angle $\pi/6$ giving 9 degrees of freedom to locate them. The location of the six points between those two lines gives 12 more degrees of freedom, and there are 16 weights making a total of 37 degrees of freedom – perhaps two more than needed. In fact, the last sample along the x axis can be locked at the edge; hence, 36 degrees of freedom are active in the final optimization, which yields a solution with 67 samples in the semi-circle (and 127 for the full circle when the integrand is not symmetric). Although the sample count is the same as that in Figure 2, the sample locations in the central region have more uniform weights and distribution, as desired.

Inspired by the results in Table 1, however, it is tempting to continue to seek a solution with fewer samples. Several effective options emerged when fourfold symmetry was explored. In this case, it is necessary to explicitly control only the Zernikes, where m is a multiple of 4, and there are 13+11+9+…+1=49 of these. The configuration at the top right in Figure 4 has four samples on the diagonal and one on the x axis that deliver 10 degrees of freedom. The 14 points between these two lines bring 42 additional degrees of freedom making a total of 52 – perhaps three more than needed. Again, one of those points ends up sitting on the boundary so only 51 degrees of freedom are active in the final optimization that yields a solution with 67 samples in the semi-circle once again. The full circle now involves 132 samples, so that configuration is only noteworthy when the integrand is symmetric.

To meet those 49 requirements for fourfold symmetry, the configuration at lower left in Figure 4 has precisely 49 degrees of freedom: 14 from the samples on the lines of symmetry and 35 from the 12 points in between (because one of those 12 ends up on the boundary). *This configuration has 65 samples in the semi-circle and 124 in the full circle, so it is a new best for both cases*. A final alternative is shown at the lower right in Figure 4 that offers 50 degrees of freedom: 30 from the location of the points along with the 20 weights. The solution once again has 65 samples in the semi-circle, but is now *another new best with 121 points for general cubature over the circle*.

Finally, on moving to two sectors where the sampling is required to be symmetric in both x and y (as in the examples in the second row in Figure 3), there are then 91 terms of the form $x^j y^k$ with even values of j and k within $j+k \le 25$ that must be controlled. (This set is interchangeable with the Zernike terms with even values of m.) Upon deleting two of the outermost points from a sector in the solution at the top left in Figure 4, there are still 92 degrees of freedom in the configuration. Upon optimizing with this reduced symmetry, the solution at the top in Figure 5 emerges. It is yet *another new best with 117 points for general cubature over the circle and 62 in the semi-circle* and is just the sort of elegant and effective solution that we sought in place of the option at the right in Figure 1 or even in Figure 2. Alternatively, starting with a square grid that has fewer samples on the y axis (while also offering 92 degrees of freedom) leads to the solution at the bottom in Figure 5. This is also a *new best with just 60 samples in the semi-circle*, which marginally beats the simple estimate in Table 1. These solutions each represent a reduction by about 25% over the corresponding numbers for the IGQ solution of Figure 1.

In summary, as we have approached it, the initial part of the challenge for any given symmetry is to find an elegant geometric pattern that delivers about the required number of degrees of freedom while smoothly melding samples near the boundary to a uniformly tiled grid away from the edge. It is quite possible, of course, that even better solutions may be found at order 25. In the case of the general cubature over the full circle, for example, it could be helpful to collapse some of the samples at the bottom in Figure 5 to sit on the y axis. (Note that each point on one of the coordinate axes generally delivers 2 degrees of freedom and represents two samples overall, while each point inside the quadrant delivers 3 degrees of freedom and represents four samples overall; hence, it offers a reduced number of degrees of freedom per sample.) With, say six on the x axis and five on the y axis and 23 points inside the first quadrant, there are then 91 degrees of freedom, which may lead to a solution with just 114 points in the circle. Such options are left for the interested reader to pursue, however, because our focus in this work is upon the semi-circle, and the second solution in Figure 5 is likely to be close to optimal for that case.

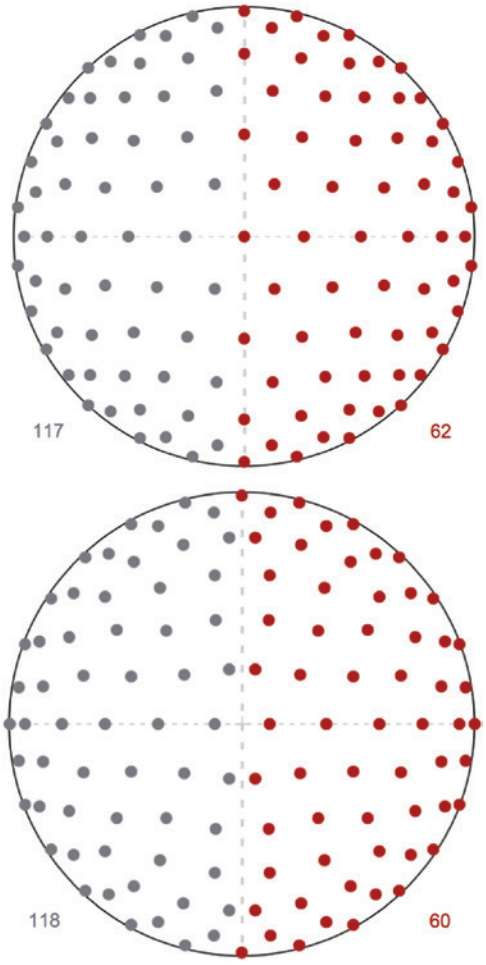

Figure 5: The more effective cubature schemes for order 25 (to be compared with those in Figures 1 and 2).

4 Lens design case study

The key component of the optical design that is of interest here involves the estimation of the RMS of the wavefront aberration, say Φ, over the pupil. In the case of lithographic projection systems, for example, the exit pupil is required to be almost perfectly circular making it an ideal application to be considered here. The patented system sketched in Figure 6 is, therefore, analyzed for

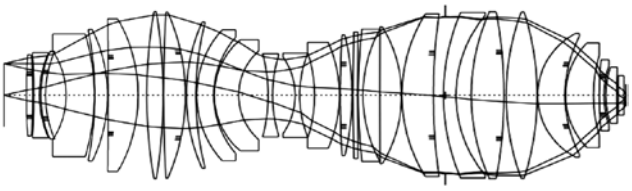

Figure 6: Section of a re-optimized system from 2003 patent #WO 03/075096 A2 (or see US 2005/0231813 A1).

demonstration. It incorporates nine aspheres (indicated by hatch marks in Figure 6) of the 16th order. Because estimates of both the mean and the mean of the square of Φ are required, it is valuable to determine how many polynomial terms are required in order to fit these functions. The results can then guide the selection of appropriate cubature schemes. Our fitting in terms of Zernike polynomials is performed by using the Ting-Luke extension of the methods presented in Ref. [5]. We use RMS normalization of the polynomials so that the fitted coefficients form a natural spectrum in that the sum of their squares equals the mean of the square of the fitted function.

For the on-axis field point of any rotationally symmetric system, just a single fan of samples is adequate to integrate over the pupil. Plots of both Φ and the amplitude of the coefficients in a Zernike polynomial fit to Φ and Φ^2 are presented in Figure 7. The absolute value of the coefficients is plotted on a logarithmic scale, where each step in the color legend corresponds to an order of magnitude change. That legend descends by four orders of magnitude from the displayed maximum value. The units are nm and nm^2 for Φ and Φ^2 in the middle and bottom rows of Figure 7, respectively. Because the mean has been subtracted from Φ, the piston term is zero in the first of these coefficient plots. In principle, all the non-zero coefficients should sit in the m=0 column, but those terms that appear in m=4 (down by a factor 0.0001) are due to interpolation off a square grid of data. Note that the dominant terms fall within say n<12 and n<16 (with m=0) for Φ and Φ^2, respectively.

As the field point moves from the axis, Φ loses its rotational symmetry. At a mid-field position, this function has the form presented in Figure 8. The dominant terms now fall within say $n+2m$<15 and $n+2m$<25 for Φ and Φ^2, respectively. Recall that the terms up to order t fill a region bounded by a slope of one half instead of two (i.e. $2n+m \le t$). This means that those two regions just mentioned contain only about one quarter of the terms of orders 30 and 50, respectively: the higher azimuthal orders are simply not significant and can, therefore, be dropped from consideration. More generally, the contours of the magnitude of the fit coefficients in Figure 8 reveal that

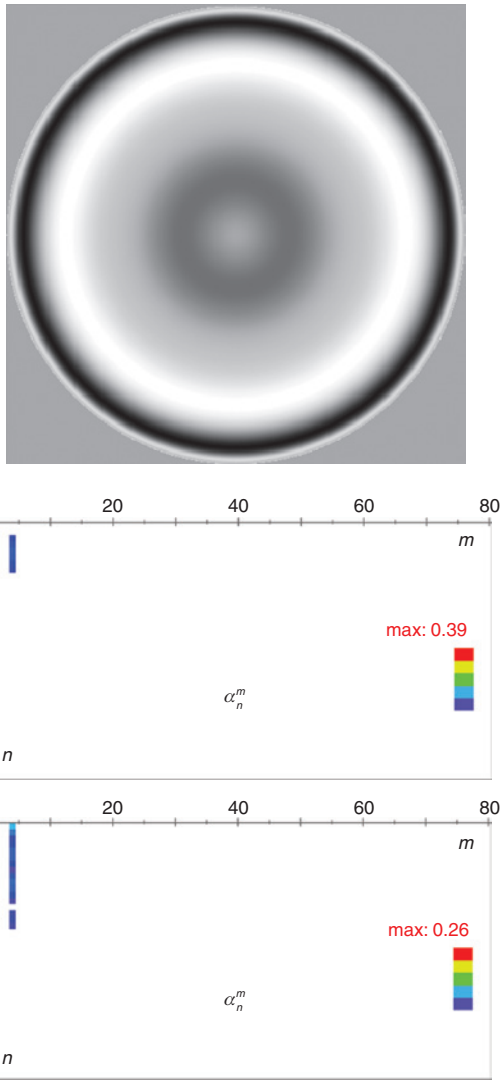

Figure 7: The wavefront aberration for the on-axis field point along with logarithmic plots of the coefficients from fits of both Φ and Φ^2 in terms of Zernike polynomials.

the slope of the truncation line should be approximately 2. That is, we should deal with all terms in a domain of the form $n+2m \le B$ for some fixed upper bound B chosen to meet the desired level of accuracy.

At the edge of the field, Φ has the form presented in Figure 9. It is worth noting that the RMS of Φ is given by the square root of the piston coefficient (namely, α_0^0) for Φ^2; all the dominant terms in that spectrum must be integrated sufficiently well to extract an accurate estimate of this RMS. The dominant terms in this case for both Φ and Φ^2 fall in regions defined roughly by $n+m \le B$. That is, the slope is now about unity, so only about one half of the terms of a fixed order are used at any likely level of truncation. Again, within the set of a given order, say $2n+m \le T$, the higher azimuthal orders are not significant, and we

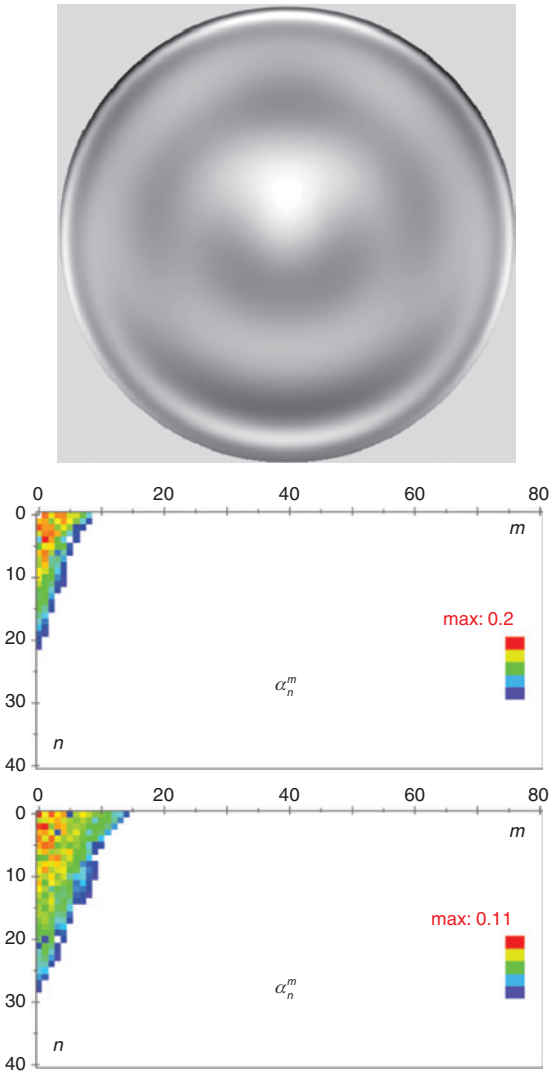

Figure 8: The wavefront aberration for the mid-field point.

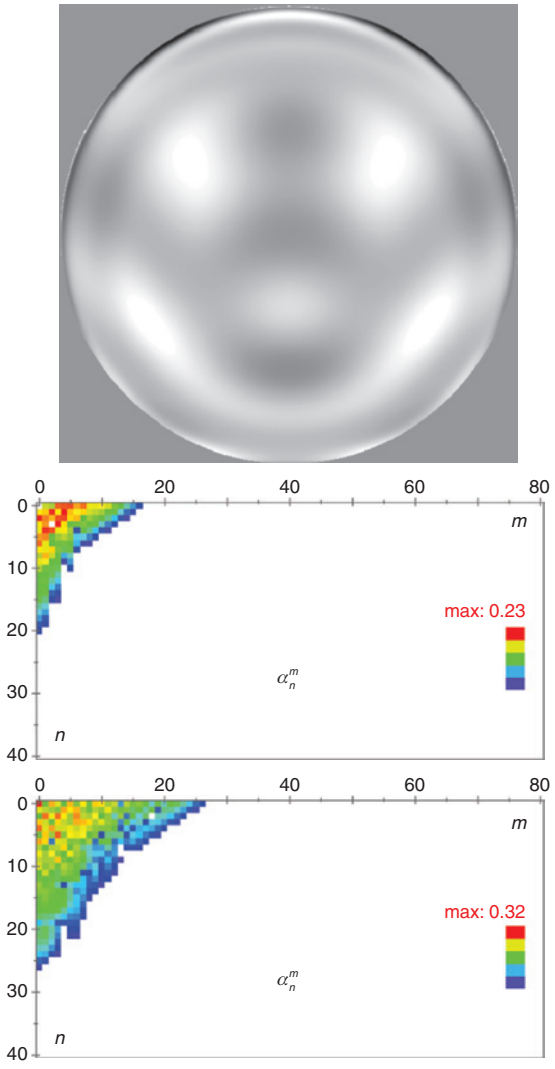

Figure 9: The wavefront aberration at the edge of the field.

need to consider only those within $2n+2m \le T$ instead. For the purposes of configuring a tailored cubature scheme, the desired level of accuracy then determines the appropriate truncation value, T.

Upon reducing the target set of polynomials in accordance with the application in hand, it can be expected that tailored cubature schemes can deliver even greater efficiency. As a first simple step in that direction for the scheme at the top left in Figure 4, consider dropping the six symmetry partners associated with the extreme point along the x axis (the vertices of the hexagon to be seen below in Figure 10). It turns out that the resulting 121 samples can be re-optimized while retaining the segmented sixfold symmetry to give exact results for all of the originally targeted Zernikes except for what is typically the least significant one, namely, $Z_0^{24}(r,\theta)$. More generally, it will not be possible to remove a sample from within a segment whenever one of the target requirements is dropped, but perhaps one for every two to three requirements that are dropped.

5 Discussion and concluding remarks

Configuring cubature schemes is an elegant design challenge that is likely to appeal to optical designers both for its clear graphical representation as well as its potential benefit in their day-to-day activities. Both design tasks are ultimately reduced to optimization problems, and it is likely that the sub-title of Ref. [2], entitled 'Configuring cubature formulae: *the science behind the art*', may also capture the eye of optical designers. As a first cut, we

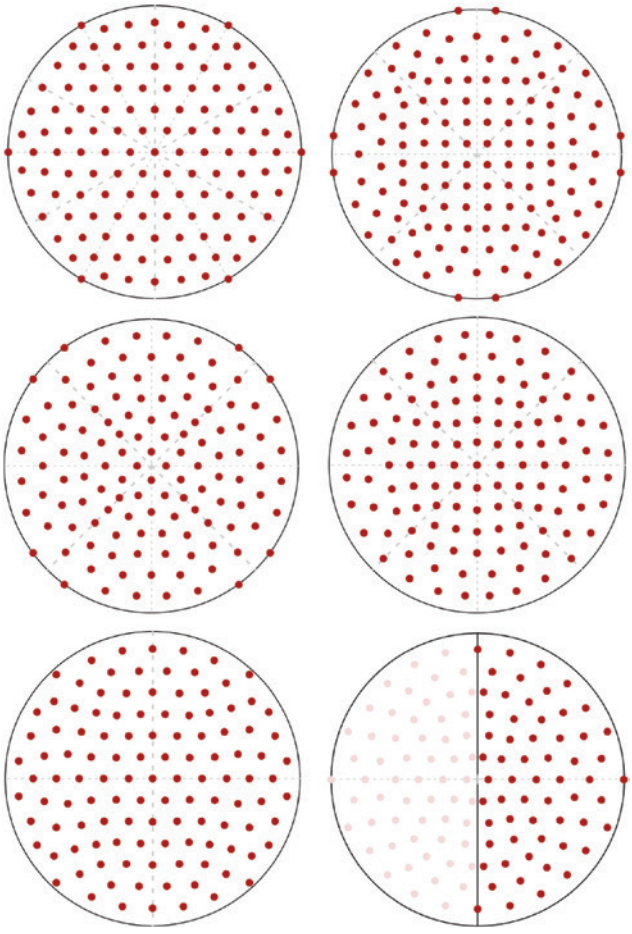

Figure 10: Insights can often be gained upon viewing the sampling patterns after warping the radial coordinate with arcsine, e.g. these plots result from Figures 4 and 5.

chose to work this problem as a local optimization task. Upon examining the solutions that emerged at different orders, we noticed that the sampling schemes appeared to be more uniform when the radial coordinate was transformed with the inverse sine function and re-normalized by dividing the result by $\pi/2$ (see Figure 10). (Keep in mind that the solution at the bottom right in Figure 10 is intended for integration over the semi-circle, so the points in the left half are dimmed.) Together with the estimated number of samples given in Table 1 and a fairly simple tiling pattern, the inverse of this transformation allowed us to configure effective starting configurations for the optimization. Of course, given the simple bounds on all parameters and the inexpensive merit function, this challenge may also be suited to global optimization.

For two-dimensional integrals, the simple estimates used for Table 1 indicate that, at higher orders, cubature may deliver a computational reduction of about 30%. When averaging is also performed over the field and spectrum (i.e. wavelength) for rotationally symmetric systems, it would appear that a four-dimensional integral is ultimately involved. If it were appropriate to retain all variables to a fixed total order, it turns out that the simple estimate based on counting terms and degrees of freedom then indicates that the computational reduction over IGQ may be by as much as 85%. [With 5 degrees of freedom per sample point and $t^4/24+O(t^3)$ terms up to order t, cubature is expected to involve about $t^4/120+O(t^3)$ samples, whereas IGQ uses about $t^4/16+O(t^3)$.] We are not so lucky, however, because the averaging over the field and color is performed on the square of the average over the aperture. This means that the aperture average cannot be combined simply with its enclosing averages. Nevertheless, it is possible in the case of polychromatic systems to also apply cubature methods to the combined field and color averages. As a result, different colors would generally be traced from the different field points, while the same pupil sampling is used for each of those combinations. It is worth noting that the remarkably effective steps introduced in Ref. [1] for the color average can be used once again to boost efficiency. Cubature may then deliver an additional reduction of 20–30% in the estimation of these outermost two integrals for a net reduction factor of about 0.75^2, i.e. by 40–50%.

Importantly, the results in Section 4 demonstrate that the pupil functions of interest in optical design are not always isotropic. There is clear reason to expect that radial (ring-like) variations are generally more dominant than azimuthal (spoke-like) patterns in the pupil of a typical rotationally symmetric system, especially those involving complex aspheres. Significant additional gains can, therefore, be expected with tailored cubature schemes that target specific collections of terms to integrate exactly. For example, in the case of the slope of unity in (m,n) index space that emerged in Section 4, perhaps an additional 40–50% reduction may ultimately be achieved when going beyond the sorts of cubature schemes presented in Section 4. Because the integrand is no longer isotropic, however, the guidance we used to find starting configurations for the optimization may no longer be as useful. We have, nevertheless, seen promising initial results of this type. Given that the associated challenges are non-trivial, it could be valuable to collect an encyclopedia akin to Ref. [4] that is targeted solely to the specific features of our optical design context.

Acknowledgments: We are grateful to Alexander Epple for the helpful discussions.

Appendix

The details for one sector for each of the cubature schemes of Section 3.2 are given here. The weights are for integrating over just the first half of the sector, so they sum to $\pi/2$ divided by the number of sectors. These points and their weights must be replicated in order to fill either the semicircle or the entire circle, so the weights for points on lines of symmetry get doubled while that for the origin is multiplied by up to twice the number of sectors. The sum of all the weights is then $\pi/2$ and π, respectively.

Top left in Figure 4 has six sectors:

j	r_j	θ_j	w_j
1	0	0	0.00503393480424
2	0.261123582247	0	0.0288540065359
3	0.504280067032	0	0.0249618271783
4	0.711375171139	0	0.0189890875003
5	0.866020646170	0	0.0117785611404
6	0.964362457335	0	0.00476733175949
7	1	0	0.000381179918233
8	0.442104616485	$\frac{\pi}{6}$	0.0262385887522
9	0.795324146927	$\frac{\pi}{6}$	0.0159857068583
10	0.983599672470	$\frac{\pi}{6}$	0.00428012878940
11	0.644299207279	0.334417464350	0.0426820266291
12	0.814663412358	0.244713343980	0.0296959857443
13	0.932380740872	0.180050986902	0.0161247936499
14	0.984652938113	0.319113581958	0.00768301591862
15	0.916251201137	0.406257777731	0.0200108931540
16	0.990727562435	0.133698702928	0.00433231946644

Top right in Figure 4 has four sectors:

j	r_j	θ_j	w_j
1	0.161879954717	$\frac{\pi}{4}$	0.0259696828670
2	0.463293256444	$\frac{\pi}{4}$	0.0223116474831
3	0.737344195914	$\frac{\pi}{4}$	0.0149750246987
4	0.967005078330	$\frac{\pi}{4}$	0.00595021250822
5	0.959078032396	0	0.00785572825901
6	0.354994579717	0.316939767168	0.0475779496797
7	0.553726177181	0.205076406284	0.0431013266784
8	0.725201039942	0.120439554078	0.0284599914743
9	0.866090777426	0.128330156482	0.0261671635242
10	1	0.128985606204	0.00287824778642
11	0.622860585686	0.557287102773	0.0390686346807
12	0.758158503588	0.368947773053	0.0296767811539
13	0.890496999145	0.379449160168	0.0219537106715
14	0.960254231346	0.234380301303	0.0139646598333
15	0.816989200535	0.591796459487	0.0217540415084
16	0.953628720661	0.535028027603	0.0142418969303
17	0.989787734718	0.393855952794	0.00615027652281
18	0.893729171019	0.683984198525	0.0165852400654
19	0.995142341224	0.640507301582	0.00405686537319

Bottom left in Figure 4 has four sectors:

j	r_j	θ_j	w_j
1	0.463814489778	$\frac{\pi}{4}$	0.0123301620651
2	0.611732085633	$\frac{\pi}{4}$	0.0158782656360
3	0.755999779643	$\frac{\pi}{4}$	0.0157218380657
4	0.964110979093	$\frac{\pi}{4}$	0.00777412404831
5	0.153752685302	0	0.0234081140212
6	0.474478358332	0	0.0227709942939
7	0.918440689571	0	0.0109734553458
8	0.337986011042	0.434127807376	0.0444836846977
9	0.667585617148	0.154560642700	0.0343476039255
10	0.985036206102	0.116440560644	0.00883065520342
11	0.558803853895	0.431556377581	0.0388306742037
12	0.738926226493	0.474657523525	0.0359190171061
13	0.814284995818	0.153827156347	0.0317176465875
14	0.932954240179	0.259204603985	0.0183741136951
15	0.865668011487	0.413395463103	0.0221722400364
16	0.958577199587	0.527781109248	0.0154568371969
17	0.989485395802	0.356542050664	0.00675527129600
18	0.877317042756	0.656904685204	0.0238728803343
19	1	0.633980031990	0.00308150394011

Bottom right in Figure 4 has four sectors. In this case, increment the angles by $\pi/4$ to obtain the geometry shown in the figure, which was rotated for purely cosmetic reasons:

j	r_j	θ_j	w_j
1	0	0	0.00733183591506
2	0.302032660355	0	0.0230949856696
3	0.575495736838	0	0.0166999321325
4	0.833508141702	0	0.0128926288985
5	0.986927317290	0	0.00413694897278
6	0.240893667941	$\frac{\pi}{4}$	0.0248931200263
7	0.461678800925	$\frac{\pi}{4}$	0.0223520334343
8	0.652823495810	$\frac{\pi}{4}$	0.0179276433554
9	0.805774504670	$\frac{\pi}{4}$	0.0148654045476
10	0.476858448510	0.322964567594	0.0427235926396
11	0.710537472994	0.171933554419	0.0318143682653
12	0.930890131030	0.131027625944	0.0188680472936
13	0.655736859341	0.463892443356	0.0370068534559
14	0.836490869680	0.264010779052	0.0235064794497
15	0.986295133846	0.248094175200	0.00841760403941
16	0.810387580848	0.512437221177	0.0293893093649
17	0.927738945961	0.397041690953	0.0195514283972
18	0.919415902805	0.653917481393	0.0216402438421
19	0.985895281633	0.483811862203	0.00799318157028
20	0.984323030577	0.691371137916	0.00759344042856

Configuration at the top in Figure 5 has two sectors:

j	r_j	θ_j	w_j
1	0	0	0.0149517568835
2	0.257965725089	0	0.0286084595777
3	0.502728284487	0	0.0250045771762
4	0.709833364782	0	0.0194802533572
5	0.855512458097	0	0.0134342864091
6	0.957499582897	0	0.00629636556408
7	0.444610654646	$\frac{\pi}{2}$	0.0260103283905
8	0.796848946153	$\frac{\pi}{2}$	0.0172170526400
9	0.982717079432	$\frac{\pi}{2}$	0.00497287778573
10	0.437873222452	0.522100899398	0.0519956502679
11	0.790589888253	0.575671654124	0.0328800015513
12	0.989231377287	0.520483893440	0.00521626068767
13	0.642192413413	0.339007064971	0.0429051232734
14	0.810258045761	0.283295793518	0.0322560049658
15	0.924872667099	0.208802147070	0.0190378409151
16	0.981314352985	0.336115318558	0.00910719735386
17	0.914863309006	0.471132006509	0.0229063431375
18	0.991572601992	0.129999285339	0.00542872482291
19	0.636382373355	0.716138034124	0.0413824741810
20	0.800297339143	0.862656545578	0.0256652550200
21	0.959014869771	0.917910427214	0.0145085021597
22	0.972938009873	0.667542285854	0.0102675125362
23	0.901728459478	0.734674579866	0.0212981409298
24	0.998441832687	0.825796382635	0.00312659972991
25	0.260798491094	1.05495455778	0.0571213915893
26	0.501041951253	1.05071964881	0.0490318985096
27	0.702535105361	1.05263833290	0.0350473688401
28	0.878961628358	1.02749621786	0.0220142356304
29	0.989268646708	1.09290883586	0.00683481864675
30	0.645535400897	1.38235622486	0.0423304142801
31	0.816074455152	1.26757789386	0.0320728140153
32	0.938225311763	1.19781755128	0.0167306892177
33	0.986459271322	1.33916501702	0.00821330767740
34	0.916486974291	1.43980472499	0.0220436356747

Configuration at the bottom in Figure 5 has two sectors:

j	r_j	θ_j	w_j
1	0.116076932388	0	0.0274076846310
2	0.361371551393	0	0.0253251898672
3	0.589951735289	0	0.0218769856445
4	0.773570576882	0	0.0162612167236
5	0.932880344724	0	0.00794880370840
6	1	0	0.00135964344870
7	0.984286770551	$\frac{\pi}{2}$	0.00495405041440
8	0.244302781461	1.33119262037	0.0325940700338
9	0.326092741109	0.705986043383	0.0466845708456
10	0.519330134060	0.407525268170	0.0451652641338
11	0.713287248840	0.296908736831	0.0378382211522
12	0.871892793483	0.186188764102	0.0267528378530
13	0.974483175564	0.163815947238	0.0117511776701
14	0.464723352232	1.32307561044	0.0464140788710
15	0.520633549191	0.888261689537	0.0414890542934
16	0.675209954505	0.642090742340	0.0381506243974
17	0.834289898767	0.464601871341	0.0295071185170
18	0.942257904761	0.387967315711	0.0188511171435
19	0.996173928937	0.354685007291	0.00402022733690
20	0.652237185112	1.38707852985	0.0416877625309
21	0.686047237660	1.03017693162	0.0399877882189
22	0.805147724545	0.751568499548	0.0275427172452
23	0.917415573879	0.663129821937	0.0215968588962
24	0.983342922913	0.583708862710	0.00951198619742
25	0.805150352736	1.50182762387	0.0196595696522
26	0.814186218117	1.25242171186	0.0301225582999
27	0.838519624239	0.983837636148	0.0245896975348
28	0.932667108176	0.908643803993	0.0178855170667
29	0.986721416556	0.816571298031	0.00816133324354
30	0.919652103297	1.43630889383	0.0221649955228
31	0.985243288879	1.31980193988	0.00939793588857
32	0.926927222250	1.17164325688	0.0201140601652
33	0.986508765698	1.06673021799	0.00862344624972

References

[1] G. W. Forbes, J. Opt. Soc. Am. A5, 1943–1956 (1988).
[2] R. Cools, Acta Numerica, 6, 1–54 (1997).
[3] R. Cools and K. J. Kim, Korean J. Comput. Appl. Math. 7, 477–485 (2000).
[4] R. Cools, J. Complexity 19, 445–453 (2003).
[5] G. W. Forbes, Opt. Exp. 21, 19061–19081 (2013).
[6] C. Menke and G. W. Forbes, Adv. Opt. Technol. 2, 97–109 (2012).

Greg W. Forbes
Physics Department, Macquarie University
North Ryde 2109, Sydney NSW, Australia
forbes@bigpond.net.au

Greg W. Forbes is an Adjunct Professor in Physics at Macquarie University (Sydney) and the Director of Scisense Consulting Pty Ltd. Following his PhD in Theoretical Physics at the Australian National University, he was a Fulbright Fellow at the Optical Sciences Center (Tucson), a tenured faculty member of The Institute of Optics (Rochester, 1985–1994), a Research Professor at Macquarie University (Sydney, 1994–2000), and a Senior Scientist at QED Technologies (2000–2015). Throughout his career, optical modeling has remained one of his primary interests.

Johannes Ruoff
Carl Zeiss SMT GmbH, Rudolf-Eber-Strasse 2
73447 Oberkochen, Germany
johannes.ruoff@zeiss.com

Johannes Ruoff is a Senior Optical Designer at Carl Zeiss SMT GmbH. He holds a PhD in Physics from the University of Tübingen, Germany. His research interests are in EUV optics, high-NA imaging, electromagnetic diffraction theory, and polarization aspects in lithography.

Andreas Flesch
Carl Zeiss AG, Carl-Zeiss-Strasse 22
73447 Oberkochen, Germany

Andreas Flesch is a staff member at the Corporate Research and Technology department at ZEISS in Oberkochen since 2013. His main research interests include optimization algorithms, mathematical surface descriptions, novel ray-based approaches for optical system modeling, and the efficient implementation of these methods in optical design software. He holds a PhD in Theoretical Physics from RWTH Aachen University, Germany.

Norbert Kerwien
Carl Zeiss AG, Carl-Zeiss-Strasse 22
73447 Oberkochen, Germany

Norbert Kerwien is the Director of the Optics Concepts group at Corporate Research and Technology of ZEISS. After his PhD on Polarization Effects in Microscopic Image Formation at the Institute of Applied Optics, University of Stuttgart, he joined the lithography division of ZEISS in 2006. Since 2010, he works at Corporate Research and Technology. Among his primary interests are physical optical image formation, computational imaging, and optical design.